Engineering Optimization
Publication details, including instructions for authors and subscription information:
http://www.tandfonline.com/loi/geno20

The continuous adjoint approach to the k-ε turbulence model for shape optimization and optimal active control of turbulent flows

E.M. Papoutsis-Kiachagias[a], A.S. Zymaris[a], I.S. Kavvadias[a], D.I. Papadimitriou[a] & K.C. Giannakoglou[a]
[a] Laboratory of Thermal Turbomachines, Parallel CFD & Optimization Unit, School of Mechanical Engineering, National Technical University of Athens, Greece
Published online: 20 Mar 2014.

To cite this article: E.M. Papoutsis-Kiachagias, A.S. Zymaris, I.S. Kavvadias, D.I. Papadimitriou & K.C. Giannakoglou (2014): The continuous adjoint approach to the k-ε turbulence model for shape optimization and optimal active control of turbulent flows, Engineering Optimization, DOI: 10.1080/0305215X.2014.892595

To link to this article: http://dx.doi.org/10.1080/0305215X.2014.892595

Engineering Optimization, 2014
http://dx.doi.org/10.1080/0305215X.2014.892595

Taylor & Francis
Taylor & Francis Group

The continuous adjoint approach to the k–ϵ turbulence model for shape optimization and optimal active control of turbulent flows

E.M. Papoutsis-Kiachagias, A.S. Zymaris, I.S. Kavvadias, D.I. Papadimitriou and K.C. Giannakoglou*

Laboratory of Thermal Turbomachines, Parallel CFD & Optimization Unit, School of Mechanical Engineering, National Technical University of Athens, Greece

(*Received 22 July 2013; accepted 22 January 2014*)

The continuous adjoint to the incompressible Reynolds-averaged Navier–Stokes equations coupled with the low Reynolds number Launder–Sharma k–ϵ turbulence model is presented. Both shape and active flow control optimization problems in fluid mechanics are considered, aiming at minimum viscous losses. In contrast to the frequently used assumption of frozen turbulence, the adjoint to the turbulence model equations together with appropriate boundary conditions are derived, discretized and solved. This is the first time that the adjoint equations to the Launder–Sharma k–ϵ model have been derived. Compared to the formulation that neglects turbulence variations, the impact of additional terms and equations is evaluated. Sensitivities computed using direct differentiation and/or finite differences are used for comparative purposes. To demonstrate the need for formulating and solving the adjoint to the turbulence model equations, instead of merely relying upon the 'frozen turbulence assumption', the gain in the optimization turnaround time offered by the proposed method is quantified.

Keywords: continuous adjoint; adjoint turbulence models; sensitivity derivatives; aerodynamic shape optimization; active flow control optimization

1. Introduction

In aerodynamic shape optimization problems, the adjoint approach remains the most efficient means of computing the sensitivity derivatives of objective functions with respect to (w.r.t.) the design variables. In either discrete (Burgreen and Baysal 1996; Elliott and Peraire 1996; Giles and Pierce 1997) or continuous form (Pironneau 1984; Jameson 1988; Anderson and Venkatakrishnan 1999; Papadimitriou and Giannakoglou 2007), it is widely used to solve aerodynamic shape optimization problems. An introduction to discrete and continuous adjoints with comments on their advantages and disadvantages can be found in Giles and Pierce (2000) and Nadarajah and Jameson (2001). The range of applications includes the inverse design of aerodynamic shapes (Jameson and Alonso 1996), the design of airfoils or wings targeting minimum drag and/or maximum or predefined lift (Reuther *et al.* 1996), sonic boom reduction (Nadarajah and Jameson 2002), the design of optimal turbomachinery cascades (Duta, Giles, and Campobasso 2002), aeroelastic optimization (Mishra *et al.* 2013), flutter suppression (Zhang *et al.* 2013), *etc*.

*Corresponding author. Email: kgianna@central.ntua.gr

In the majority of articles on the continuous adjoint to the Reynolds-averaged Navier–Stokes (RANS) equations for turbulent flows (Anderson and Venkatakrishnan 1999; Jameson, Pierce, and Martinelli 1998; Papadimitriou and Giannakoglou 2007; Othmer 2008) all variations in turbulent quantities w.r.t. the design variables are neglected, a simplification that is often referred to as the 'frozen turbulence' assumption. This is not usually the case in the discrete adjoint approach where the turbulence model equations are linearized, thus allowing the computation of exact sensitivity derivatives (Anderson and Bonhaus 1999; Nielsen *et al.* 2004; Lee and Kim 2007; Dwight, Brézillon, and Vollmer 2006). This process can be greatly facilitated by using Algorithmic Differentiation (AD) (Naumann 2012; Nemili *et al.* 2013). In contrast, regarding the continuous to the RANS equations, adjoint method, there are just a few recent articles which compute exact sensitivities without making the 'frozen turbulence' assumption. In Zymaris *et al.* (2009), the adjoint to the Spalart–Allmaras one-equation turbulence model for incompressible flows was presented, addressing the differentiation of turbulence models with the continuous adjoint method for the first time in the literature. Later on, the exact continuous adjoint approach to compressible flows based on the same turbulence model was also presented (Bueno-Orovio *et al.* 2012). In Zymaris *et al.* (2010), the adjoint approach to the high-Reynolds k–ϵ turbulence model with wall functions was formulated by introducing the adjoint friction velocity and the so-called adjoint wall functions. A hybrid adjoint method, in which the continuous adjoint mean flow equations are combined with the discrete adjoint turbulence model, was presented in Taylor *et al.* (2013).

During the last years, the adjoint method has also been used in the optimization of flow control systems. It is known that active flow control, based on suction or blowing jets, can successfully control boundary layer development (Prandtl 1904). Jets may control the boundary layer, prevent or delay separation, suppress or enhance turbulence, control shock waves, *etc*. The adjoint technique has been used in the framework of gradient-based optimization methods to determine the optimal characteristics of steady and unsteady flow control jets (Joslin *et al.* 1997; Cathalifaud and Luchini 2000; He *et al.* 2000; Pralits, Hanifi, and Henningson 2002; Li *et al.* 2003; Collis *et al.* 2004; Carnarius *et al.* 2013; Nemili *et al.* 2013). Zymaris *et al.* (2013) presented the continuous adjoint approach to flow control problems governed by the Spalart–Allmaras turbulence model for incompressible flows. The adjoint method computes the sensitivity derivatives of the objective function w.r.t. the hypothetical normal jet volume flow rate at the wall grid faces. Then, the jet locations with the highest potential for improvement are identified based on the magnitude of the computed sensitivities and the jet 'type' is chosen according to their signs.

This article relies upon the Launder–Sharma k–ϵ turbulence model for incompressible flows. This article aims at:

- formulating the continuous adjoint approach to the Launder–Sharma k–ϵ model PDEs, for the first time in the relevant literature, and identifying extra terms in the adjoint meanflow PDEs, their boundary conditions and the sensitivity derivatives,
- conducting numerical tests in both shape and active flow control optimization, proving the accuracy of the computed objective function gradient, in contrast to the lack of accuracy in computations following the 'frozen turbulence' assumption, and
- presenting comparisons showing that, with the present method, the overall optimization turnaround time reduces if the adjoint to the turbulence model equations are solved.

Although a single objective function (the difference in the volume-averaged total pressure between the domain inlet and outlet) is analysed, the development is general and can be adapted to other objective functions, such as those used by the authors in previous publications (Papadimitriou and Giannakoglou 2007, 2012; Zymaris *et al.* 2013). Regarding the need to differentiate the k–ϵ PDEs, this article reconfirms findings for the one-equation turbulence model published in Zymaris *et al.* (2009), in an attempt to generalize them to other turbulence models. The selection

of this particular variant of the k–ϵ model here implies neither the authors' preference for it nor its superiority with respect to other turbulence models in use. It is, however, a widely used turbulence model, especially in internal aerodynamics. Any other k–ϵ model variant could be used instead. Compared to Spalart–Allmaras (and its adjoint formulation, Zymaris *et al.* [2009]), the Launder–Sharma k–ϵ model does not depend exclusively on the distance of internal nodes from the solid walls, making the derivation of the adjoint equations free of relevant issues (Bueno-Orovio *et al.* 2012). However, the Launder–Sharma k–ϵ model includes nonlinear combinations of high-order spatial derivative terms which lead to up to fourth-order spatial derivatives in the adjoint formulation.

2. State equations

The incompressible flow model consists of the RANS equations coupled with the low-Re number Launder–Sharma k–ϵ turbulence model (Launder and Sharma 1974). The mean-flow equations are given by

$$R^p = -\frac{\partial v_j}{\partial x_j} = 0 \tag{1a}$$

$$R_i^v = v_j \frac{\partial v_i}{\partial x_j} - \frac{\partial}{\partial x_j}\left[(\nu + \nu_t)\left(\frac{\partial v_i}{\partial x_j} + \frac{\partial v_j}{\partial x_i}\right)\right] + \frac{\partial p}{\partial x_i} = 0, \quad i = 1, 2(, 3), \tag{1b}$$

where v_i are the velocity components, p is the static pressure divided by the constant density, ν is the constant bulk viscosity and ν_t is the turbulent viscosity. In what follows, the Einstein convention, where repeated indices imply summation, is used unless stated otherwise. The Launder–Sharma k–ϵ turbulence model is expressed by the following system of PDEs:

$$R^k = v_j \frac{\partial k}{\partial x_j} - \frac{\partial}{\partial x_j}\left[\left(\nu + \frac{\nu_t}{\mathrm{Pr}_k}\right)\frac{\partial k}{\partial x_j}\right] - P_k + \epsilon + D = 0 \tag{2a}$$

$$R^\epsilon = v_j \frac{\partial \epsilon}{\partial x_j} - \frac{\partial}{\partial x_j}\left[\left(\nu + \frac{\nu_t}{\mathrm{Pr}_\epsilon}\right)\frac{\partial \epsilon}{\partial x_j}\right] - c_1 P_k \frac{\epsilon}{k} + c_2 f_2 \frac{\epsilon^2}{k} - E = 0. \tag{2b}$$

The eddy viscosity coefficient ν_t depends on the turbulent kinetic energy k and the turbulent energy dissipation ϵ as follows:

$$\nu_t = c_\mu f_\mu \frac{k^2}{\epsilon}, \tag{3}$$

where the model constants are $c_\mu = 0.09$, $c_1 = 1.44$, $c_2 = 1.92$, $\mathrm{Pr}_k = 1.0$ and $\mathrm{Pr}_\epsilon = 1.3$. The production term P_k and the low-Re number terms D and E are given by

$$P_k = \nu_t P, \quad P = \left(\frac{\partial v_i}{\partial x_j} + \frac{\partial v_j}{\partial x_i}\right)\frac{\partial v_i}{\partial x_j}, \quad D = 2\nu\left(\frac{\partial(\sqrt{k})}{\partial x_j}\right)^2, \quad E = 2\nu\nu_t\left(\frac{\partial^2 v_k}{\partial x_i \partial x_j}\right)^2. \tag{4}$$

Also,

$$f_\mu = \exp\left[\frac{-3.4}{\left(1 + \frac{\mathrm{Re}_t}{50}\right)^2}\right], \quad f_2 = 1 - 0.3\exp\left[-\min(\mathrm{Re}_t^2, 50)\right], \tag{5}$$

where $\mathrm{Re}_t = k^2/\nu\epsilon$.

As discussed in the introduction, compared to the Spalart–Allmaras model and the corresponding continuous adjoint formulation in Zymaris *et al.* (2009), the k–ϵ model does not include terms depending on distances from the walls; the differentiation of the latter might become an extra burden and, depending on the approach, a source of error.

The flow equations are solved using a cell-centred, collocated finite-volume scheme. The mean-flow equations are solved in a segregated manner by employing the SIMPLE algorithm (Patankar and Spalding 1972), and the solution of the turbulence model PDEs is decoupled.

3. The objective function and its differentiation

In general, an objective function defined along the boundaries S (or part of them) of the computational domain Ω can be expressed as

$$F = \int_S F_{S_i} n_i \, \mathrm{d}S, \tag{6}$$

where the integrand depends on the outwards-facing, unit normal vector $\mathbf{n}$. F_{S_i} may or may not include turbulence variables, such as k, ϵ or ν_t. To keep the notation as simple as possible and since only an objective function defined at the boundaries of the computational domain is investigated in this article, no volume (Ω) integral is added to the right-hand side of Equation (6), as in Papadimitriou and Giannakoglou (2007). S can be decomposed into $S = S_I \cup S_O \cup S_W$, where S_I, S_O and S_W are the inlet, outlet and wall boundaries of Ω, respectively.

F should be differentiated w.r.t. the design variables b_m, $m \in [1, N]$. In this context, variations in any quantity Φ (standing for any flow variable or F_{S_i}) along the boundary S can written as (Grinfield 2010)

$$\frac{\delta \Phi}{\delta b_m} = \frac{\partial \Phi}{\partial b_m} + \frac{\partial \Phi}{\partial x_k} n_k \frac{\delta x_l}{\delta b_m} n_l. \tag{7}$$

In Equation (7), $\delta\Phi/\delta b_m$ denotes the total derivative of any quantity Φ and represents the total change in Φ caused by variations in b_m. The partial derivative $\partial\Phi/\partial b_m$ represents the variation in Φ caused purely by changes in the flow variables (in turn, caused by the geometry deformation) without considering space deformations. In flow control optimization problems, where the design variables are hypothetical jet volume flow rates at the (perforated) wall boundaries, $\delta x_k/\delta b_m$ is zero and Equation (7) becomes

$$\frac{\delta \Phi}{\delta b_m} = \frac{\partial \Phi}{\partial b_m}.$$

The continuous adjoint formulation, as presented below, primarily focuses on shape optimization problems and is then adapted to flow control optimization in Section 4.4.

In shape optimization, only wall boundaries are allowed to deform. By taking into consideration Equation (7), and by applying the chain rule for the partial derivative of F, we get

$$\begin{aligned}\frac{\delta F}{\delta b_m} = &\int_S \frac{\partial F_{S_i}}{\partial v_k} n_i \frac{\partial v_k}{\partial b_m} \mathrm{d}S + \int_S \frac{\partial F_{S_i}}{\partial p} n_i \frac{\partial p}{\partial b_m} \mathrm{d}S + \int_S \frac{\partial F_{S_i}}{\partial k} n_i \frac{\partial k}{\partial b_m} \mathrm{d}S + \int_S \frac{\partial F_{S_i}}{\partial \epsilon} n_i \frac{\partial \epsilon}{\partial b_m} \mathrm{d}S \\ &+ \int_S \frac{\partial F_{S_i}}{\partial \tau_{kj}} n_i \frac{\partial \tau_{kj}}{\partial b_m} \mathrm{d}S + \int_{S_w} n_i \frac{\partial F_{S_{W,i}}}{\partial x_k} n_k \frac{\delta x_l}{\delta b_m} n_l \, \mathrm{d}S + \int_{S_w} F_{S_i} \frac{\delta n_i}{\delta b_m} \mathrm{d}S + \int_{S_w} F_{S_i} n_i \frac{\delta(\mathrm{d}S)}{\delta b_m},\end{aligned} \tag{8}$$

where

$$\tau_{kj} = (\nu + \nu_t) \left(\frac{\partial v_k}{\partial x_j} + \frac{\partial v_j}{\partial x_k} \right)$$

is the stress tensor.

If the partial derivatives $\partial/\partial b_m$ of the flow variables were to be computed, N systems of equations, similar in complexity to the primal ones, would have to be solved. Such a costly procedure is referred to as 'Direct Differentiation' (DD). In what follows, DD is used alongside Finite Differences (FD) to compute 'reference' sensitivities. To avoid the cost of the DD method, which may become excessive if N is very large, the (continuous) adjoint method is used.

4. The continuous adjoint method

4.1. *Formulation*

The starting point of the continuous adjoint formulation is the augmented objective function, defined by adding to F the volume integral of the primal equations multiplied by the corresponding adjoint variables as follows:

$$F_{\text{aug}} = F + \int_\Omega u_i R_i^v \,\mathrm{d}\Omega + \int_\Omega q R^p \,\mathrm{d}\Omega + \int_\Omega k_a R^k \,\mathrm{d}\Omega + \int_\Omega \epsilon_a R^\epsilon \,\mathrm{d}\Omega. \tag{9}$$

Apart from the adjoint velocities and pressure, u_i and q, Equation (9) also includes the adjoint to the turbulence kinetic energy and energy dissipation (k_a and ϵ_a, respectively). The latter are neglected in the commonly used 'frozen turbulence' assumption, with a certain loss in accuracy, as discussed in Section 5.

By differentiating w.r.t. b_m and employing the Leibniz theorem for integrals with varying boundaries ($S = S(\mathbf{b})$), we get

$$\begin{aligned}\frac{\delta F_{\text{aug}}}{\delta b_m} = \frac{\delta F}{\delta b_m} &+ \int_\Omega u_i \frac{\partial R_i^v}{\partial b_m}\,\mathrm{d}\Omega + \int_\Omega q \frac{\partial R^p}{\partial b_m}\,\mathrm{d}\Omega + \int_\Omega k_a \frac{\partial R^k}{\partial b_m}\,\mathrm{d}\Omega + \int_\Omega \epsilon_a \frac{\partial R^\epsilon}{\partial b_m}\,\mathrm{d}\Omega \\ &+ \int_S \left(u_i R_i^v + q R^p + k_a R^k + \epsilon_a R^\epsilon\right) n_k \frac{\delta x_k}{\delta b_m}\,\mathrm{d}S.\end{aligned} \tag{10}$$

Assuming constant bulk viscosity ν, the partial derivatives of the mean-flow and turbulence model equations, Equations (1) and (2) , w.r.t. b_m yield

$$\frac{\partial R^p}{\partial b_m} = -\frac{\partial}{\partial x_j}\left(\frac{\partial v_j}{\partial b_m}\right) \tag{11}$$

$$\begin{aligned}\frac{\partial R_i^v}{\partial b_m} = &\frac{\partial v_j}{\partial b_m}\frac{\partial v_i}{\partial x_j} + v_j \frac{\partial}{\partial x_j}\left(\frac{\partial v_i}{\partial b_m}\right) + \frac{\partial}{\partial x_i}\left(\frac{\partial p}{\partial b_m}\right) \\ &- \frac{\partial}{\partial x_j}\left\{(\nu+\nu_t)\left[\frac{\partial}{\partial x_j}\left(\frac{\partial v_i}{\partial b_m}\right) + \frac{\partial}{\partial x_i}\left(\frac{\partial v_j}{\partial b_m}\right)\right]\right\} \underbrace{- \frac{\partial}{\partial x_j}\left[\frac{\partial \nu_t}{\partial b_m}\left(\frac{\partial v_i}{\partial x_j} + \frac{\partial v_j}{\partial x_i}\right)\right]}_{T_{T_i}}\end{aligned} \tag{12}$$

$$\begin{aligned}\frac{\partial R^k}{\partial b_m} = &\frac{\partial v_j}{\partial b_m}\frac{\partial k}{\partial x_j} + v_j \frac{\partial}{\partial x_j}\left(\frac{\partial k}{\partial b_m}\right) - \frac{\partial}{\partial x_j}\left[\left(\nu + \frac{\nu_t}{\mathrm{Pr}_k}\right)\frac{\partial}{\partial x_j}\left(\frac{\partial k}{\partial b_m}\right)\right] \\ &- \frac{1}{\mathrm{Pr}_k}\frac{\partial}{\partial x_j}\left(\frac{\partial \nu_t}{\partial b_m}\frac{\partial k}{\partial x_j}\right) - \frac{\partial P_k}{\partial b_m} + \frac{\partial \epsilon}{\partial b_m} + \frac{\partial D}{\partial b_m}\end{aligned} \tag{13}$$

$$\frac{\partial R^{\epsilon}}{\partial b_m} = \frac{\partial v_j}{\partial b_m}\frac{\partial \epsilon}{\partial x_j} + v_j\frac{\partial}{\partial x_j}\left(\frac{\partial \epsilon}{\partial b_m}\right) - \frac{\partial}{\partial x_j}\left[\left(\nu + \frac{\nu_t}{\mathrm{Pr}_\epsilon}\right)\frac{\partial}{\partial x_j}\left(\frac{\partial \epsilon}{\partial b_m}\right)\right]\frac{1}{\mathrm{Pr}_\epsilon}\frac{\partial}{\partial x_j}\left(\frac{\partial \nu_t}{\partial b_m}\frac{\partial \epsilon}{\partial x_j}\right)$$
$$- c_1\frac{\partial P_k}{\partial b_m}\frac{\epsilon}{k} - c_1 P_k\frac{1}{k}\frac{\partial \epsilon}{\partial b_m} + c_1 P_k\frac{\epsilon}{k^2}\frac{\partial k}{\partial b_m} + 2c_2 f_2\frac{\epsilon}{k}\frac{\partial \epsilon}{\partial b_m}$$
$$- c_2 f_2\frac{\epsilon^2}{k^2}\frac{\partial k}{\partial b_m} + c_2\frac{\epsilon^2}{k}\frac{\partial f_2}{\partial b_m} - \frac{\partial E}{\partial b_m}, \tag{14}$$

where T_{T_i} are absent in the 'frozen turbulence' adjoint formulation.
The differentiation of ν_t yields

$$\frac{\partial \nu_t}{\partial b_m} = c_\mu\frac{\partial f_\mu}{\partial b_m}\frac{k^2}{\epsilon} + 2c_\mu f_\mu\frac{k}{\epsilon}\frac{\partial k}{\partial b_m} - c_\mu f_\mu\frac{k^2}{\epsilon^2}\frac{\partial \epsilon}{\partial b_m} = B_1\frac{\partial k}{\partial b_m} + B_2\frac{\partial \epsilon}{\partial b_m}. \tag{15}$$

Based on a mathematical development employing the Green–Guass theorem, which is omitted in the interests of space, Equation (10) becomes

$$\frac{\delta F_{\mathrm{aug}}}{\delta b_m} = \int_S BC_i^q\frac{\partial v_i}{\partial b_m}\,\mathrm{d}S + \int_S (u_j n_j + \frac{\partial F_{S_i}}{\partial p}n_i)\frac{\partial p}{\partial b_m}\,\mathrm{d}S + \int_S BC^{k_a}\frac{\partial k}{\partial b_m}\,\mathrm{d}S + \int_S BC^{\epsilon_a}\frac{\partial \epsilon}{\partial b_m}\,\mathrm{d}S$$
$$+ \int_S (-u_i n_j + \frac{\partial F_{S_k}}{\partial \tau_{ij}}n_k)\frac{\partial \tau_{ij}}{\partial b_m}\,\mathrm{d}S - \int_S k_a\left(\nu + \frac{\nu_t}{\mathrm{Pr}_k}\right)\frac{\partial}{\partial b_m}\left(\frac{\partial k}{\partial x_j}\right)n_j\,\mathrm{d}S$$
$$- \int_S \epsilon_a\left(\nu + \frac{\nu_t}{\mathrm{Pr}_\epsilon}\right)\frac{\partial}{\partial b_m}\left(\frac{\partial \epsilon}{\partial x_j}\right)n_j\,\mathrm{d}S - \int_S 4\epsilon_a\nu\nu_t\frac{\partial^2 v_k}{\partial x_i\partial x_j}\frac{\partial}{\partial x_j}\left(\frac{\partial v_k}{\partial b_m}\right)n_i\,\mathrm{d}S$$
$$+ \int_\Omega R_i^u\frac{\partial v_i}{\partial b_m}\,\mathrm{d}\Omega + \int_\Omega R^q\frac{\partial p}{\partial b_m}\,\mathrm{d}\Omega + \int_\Omega R^{k_a}\frac{\partial k}{\partial b_m}\,\mathrm{d}\Omega + \int_\Omega R^{\epsilon_a}\frac{\partial \epsilon}{\partial b_m}\,\mathrm{d}\Omega$$
$$+ \int_{S_w} n_i\frac{\partial F_{S_i}}{\partial x_m}n_m\frac{\delta x_k}{\delta b_m}n_k\,\mathrm{d}S + \int_{S_w} F_{S_i}\frac{\delta n_i}{\delta b_m}\,\mathrm{d}S + \int_{S_w} F_{S_i}n_i\frac{\delta(\mathrm{d}S)}{\delta b_m}$$
$$+ \int_{S_w} (u_i R_i^v + qR^p + k_a R^k + \epsilon_a R^\epsilon)\frac{\delta x_k}{\delta b_m}n_k\,\mathrm{d}S, \tag{16}$$

where R_i^u, R^q, R^{k_a}, R^{ϵ_a}, BC_i^q, BC^{k_a} and BC^{ϵ_a} are defined in what follows.

4.2. *Field adjoint equation*

In Equation (16), field integrals which include $\partial v_i/\partial b_m$ and $\partial p/\partial b_m$ are eliminated by satisfying the adjoint to the mean-flow equations,

$$R^q = -\frac{\partial u_j}{\partial x_j} = 0 \tag{17}$$

$$R_i^u = u_j\frac{\partial v_j}{\partial x_i} - \frac{\partial(v_j u_i)}{\partial x_j} - \frac{\partial}{\partial x_j}\left[(\nu + \nu_t)\left(\frac{\partial u_i}{\partial x_j} + \frac{\partial u_j}{\partial x_i}\right)\right] + \frac{\partial q}{\partial x_i}$$
$$\underbrace{+ k_a\frac{\partial k}{\partial x_i} + \epsilon_a\frac{\partial \epsilon}{\partial x_i} + 2\frac{\partial}{\partial x_j}\left[\left(k_a + \epsilon_a c_1\frac{\epsilon}{k}\right)\nu_t\left(\frac{\partial v_i}{\partial x_j} + \frac{\partial v_j}{\partial x_i}\right)\right] - 4\frac{\partial^2}{\partial x_l\partial x_j}\left(\epsilon_a\nu\nu_t\frac{\partial^2 v_i}{\partial x_l\partial x_j}\right)}_{A1}$$
$$= 0, \quad i = 1, 2(, 3), \tag{18}$$

where $A1$ stands for the extra terms in the adjoint momentum equations, resulting from the differentiation of the turbulence model. These terms depend, among other things, on k_a and ϵ_a, and do not exist in the 'frozen turbulence' formulation.

In Equation (16), volume integrals which include $\partial k/\partial b_m$ and $\partial \epsilon/\partial b_m$ are eliminated by satisfying the adjoint turbulence model PDEs, which are

$$\begin{aligned} R^{k_a} = &-\frac{\partial (v_j k_a)}{\partial x_j} - \frac{\partial}{\partial x_j}\left[\left(\nu + \frac{\nu_t}{\mathrm{Pr}_k}\right)\frac{\partial k_a}{\partial x_j}\right] + B_1\left(\frac{\partial v_i}{\partial x_j} + \frac{\partial v_j}{\partial x_i}\right)\frac{\partial u_i}{\partial x_j} \\ &+ \left(\frac{B_1}{\mathrm{Pr}_k} - \frac{\nu}{k}\right)\frac{\partial k}{\partial x_j}\frac{\partial k_a}{\partial x_j} + \frac{B_1}{\mathrm{Pr}_\epsilon}\frac{\partial \epsilon}{\partial x_j}\frac{\partial \epsilon_a}{\partial x_j} + \left[\frac{\nu}{2k^2}\left(\frac{\partial k}{\partial x_j}\right)^2 - \frac{\nu}{k}\frac{\partial^2 k}{\partial x_j^2} - PB_1\right]k_a \\ &- \left[c_1\frac{\epsilon}{k}PB_1 + 2\nu\left(\frac{\partial^2 v_k}{\partial x_i \partial x_j}\right)^2 B_1 + c_2 f_2 \frac{\epsilon^2}{k^2} - 1\cdot 2c_2\frac{k^2}{\nu^2}e^{-\mathrm{Re}_t^2} - c_1 P_k\frac{\epsilon}{k^2}\right]\epsilon_a = 0 \end{aligned} \tag{19}$$

$$\begin{aligned} R^{\epsilon_a} = &-\frac{\partial (v_j \epsilon_a)}{\partial x_j} - \frac{\partial}{\partial x_j}\left[\left(\nu + \frac{\nu_t}{\mathrm{Pr}_\epsilon}\right)\frac{\partial \epsilon_a}{\partial x_j}\right] \\ &+ B_2\left(\frac{\partial v_i}{\partial x_j} + \frac{\partial v_j}{\partial x_i}\right)\frac{\partial u_i}{\partial x_j} + \frac{B_2}{\mathrm{Pr}_\epsilon}\frac{\partial \epsilon}{\partial x_j}\frac{\partial \epsilon_a}{\partial x_j} + \frac{B_2}{\mathrm{Pr}_k}\frac{\partial k}{\partial x_j}\frac{\partial k_a}{\partial x_j} + (1 - PB_2)\,k_a \\ &+ \left[-2\nu\left(\frac{\partial^2 v_k}{\partial x_i \partial x_j}\right)^2 B_2 - c_1\frac{\epsilon}{k}PB_2 + 2c_2 f_2\frac{\epsilon}{k} - 0.6c_2\frac{k^3}{\nu^2\epsilon}e^{-\mathrm{Re}_t^2} - c_1 P_k\frac{1}{k}\right]\epsilon_a = 0. \end{aligned} \tag{20}$$

Similarly to the turbulence production term P in Equation (4), the term

$$\left(\frac{\partial v_i}{\partial x_j} + \frac{\partial v_j}{\partial x_i}\right)\frac{\partial u_i}{\partial x_j}$$

(Equations 19 and 20) can be seen as the adjoint turbulence production which links the adjoint mean flow to the adjoint turbulence PDEs. In contrast to P, the adjoint turbulence production term is linear.

4.3. *Adjoint boundary conditions*

The boundary conditions for the adjoint variables are derived from Equation (16) by eliminating variations in the mean flow and turbulence model variables along S_I, S_O and S_W.

Along the inlet S_I, the first, third and fourth integrals in Equation (16) vanish automatically due to the Dirichlet conditions imposed on v_i, k and ϵ. The second and fifth integrals in Equation (16), written along S_I, are eliminated by setting

$$u_j n_j = u_{\langle n \rangle} = -\frac{\partial F_{S_{I,j}}}{\partial p} n_i \tag{21a}$$

$$u_i t_i^I = u_{\langle t \rangle}^I = \frac{\partial F_{S_{I,k}}}{\partial \tau_{ij}} n_k t_i^I n_j + \frac{\partial F_{S_{I,k}}}{\partial \tau_{ij}} n_k t_j^I n_i \tag{21b}$$

$$u_i t_i^{II} = u_{\langle t \rangle}^{II} = \frac{\partial F_{S_{I,k}}}{\partial \tau_{ij}} n_k t_i^{II} n_j + \frac{\partial F_{S_{I,k}}}{\partial \tau_{ij}} n_k t_j^{II} n_i, \tag{21c}$$

where t_i^I and t_i^{II} are the two components (in $3D$ cases) of the tangent to the surface unit vectors. The first tangent vector t_i^I can be defined arbitrarily whereas $t_i^{II} = e_{ijk} n_j t_k^I$, where e_{ijk} is the permutation symbol. In order to make Equation (16) independent of

$$\frac{\partial}{\partial b_m}\left(\frac{\partial k}{\partial x_j}\right) n_j \quad \text{and} \quad \frac{\partial}{\partial b_m}\left(\frac{\partial \epsilon}{\partial x_j}\right) n_j$$

along S_I, the conditions $k_a = 0$ and $\epsilon_a = 0$ are imposed.

Regarding the outlet S_O, the second, sixth and seventh integrals in Equation (16), written along S_O, vanish automatically due to the boundary conditions of p, k and ϵ. Assuming an almost uniform velocity profile at the outlet, the fifth and eighth integrals in Equation (16) vanish too.

In order to make Equation (16) independent of $\partial k/\partial b_m$ and $\partial \epsilon/\partial b_m$, the following Robin type boundary conditions for k_a and ϵ_a must be satisfied along S_O:

$$\begin{aligned} BC^{k_a} &= -\left[\left(\frac{B_1}{\mathrm{Pr}_k}-\frac{\nu}{k}\right)\frac{\partial k}{\partial x_j}n_j-\nu_j n_j\right]k_a+\left(\nu+\frac{\nu_t}{\mathrm{Pr}_k}\right)\frac{\partial k_a}{\partial x_j}n_j-\frac{B_1}{\mathrm{Pr}_\epsilon}\frac{\partial \epsilon}{\partial x_j}n_j\epsilon_a+\frac{\partial F_{S,i}}{\partial k}n_i \\ &= \nu_{\langle n\rangle}k_a+\left(\nu+\frac{\nu_t}{\mathrm{Pr}_k}\right)\frac{\partial k_a}{\partial n}+\frac{\partial F_{S,i}}{\partial k}n_i=0 \end{aligned} \tag{22}$$

$$\begin{aligned} BC^{\epsilon_a} &= -\left[\frac{B_2}{\mathrm{Pr}_\epsilon}\frac{\partial \epsilon}{\partial x_j}n_j-\nu_j n_j\right]\epsilon_a+\left(\nu+\frac{\nu_t}{\mathrm{Pr}_\epsilon}\right)\frac{\partial \epsilon_a}{\partial x_j}n_j-\frac{B_2}{\mathrm{Pr}_k}\frac{\partial k}{\partial x_j}n_j k_a+\frac{\partial F_{S,i}}{\partial \epsilon}n_i \\ &= \nu_{\langle n\rangle}\epsilon_a+\left(\nu+\frac{\nu_t}{\mathrm{Pr}_\epsilon}\right)\frac{\partial \epsilon_a}{\partial n}+\frac{\partial F_{S,i}}{\partial \epsilon}n_i=0. \end{aligned} \tag{23}$$

Equation (16) becomes independent of $\partial v_i/\partial b_m$ by satisfying

$$\begin{aligned} BC_i^q &= u_i v_j n_j+(\nu+\nu_t)\left(\frac{\partial u_i}{\partial x_j}+\frac{\partial u_j}{\partial x_i}\right)n_j-qn_i+\frac{\partial F_{S_k}}{\partial v_i}n_k \\ &\underbrace{-4\frac{\partial}{\partial x_k}\left(\epsilon_a\nu\nu_t\frac{\partial^2 v_i}{\partial x_k\partial x_j}\right)n_j-2\left(k_a+\epsilon_a c_1\frac{\epsilon}{k}\right)\nu_t\frac{\partial v_i}{\partial x_j}n_j}_{A2}=0, \quad i=1,2(,3). \end{aligned} \tag{24}$$

Eqation (24) includes the terms $A2$ which result from the differentiation of the turbulence model equations. The significance of these terms is investigated in Section 5. In 2D (3D) problems, Equation (24) includes three (four) unknown variables: of the two (three) components of the adjoint velocity and the adjoint pressure, one of them, $u_{\langle n\rangle}$, is extrapolated from the interior of the domain.

Finally, since the boundary condition types for the primal quantities are the same for both S_I and S_W (Dirichlet conditions for v_i, k and ϵ and a zero Neumann condition for p), the adjoint boundary conditions are the same too. In Equations (21), it suffices to replace $F_{S_{I,i}}$ with $F_{S_{W,i}}$. In shape optimization, since the wall shape is controlled ($\delta x_k/\delta b_m \neq 0$), these conditions give rise to extra terms to be added to the sensitivity derivatives expression, as presented in Section 4.4.

4.4. *Sensitivity derivatives*

After satisfying the field adjoint equations and their boundary conditions, the sensitivity derivatives for shape optimization are computed through

$$\begin{aligned} \frac{\delta F}{\delta b_m} &= -\int_{S_W}\left[\nu\left(\frac{\partial u_i}{\partial x_j}+\frac{\partial u_j}{\partial x_i}\right)n_j-qn_i+\frac{\partial F_{S_{W,k}}}{\partial v_i}n_k\right]\frac{\partial v_i}{\partial x_z}n_z\frac{\delta x_l}{\delta b_m}n_l\,\mathrm{d}S \\ &\underbrace{-\int_{S_W}\left(\nu\frac{\partial k_a}{\partial n}+\frac{\partial F_{S_{W,i}}}{\partial k}n_i\right)\frac{\partial k}{\partial n}\frac{\delta x_k}{\delta b_m}n_k\,\mathrm{d}S-\int_{S_W}\left(\nu\frac{\partial \epsilon_a}{\partial n}+\frac{\partial F_{S_{W,i}}}{\partial \epsilon}n_i\right)\frac{\partial \epsilon}{\partial n}\frac{\delta x_k}{\delta b_m}n_k\,\mathrm{d}S}_{B}+T_D, \end{aligned} \tag{25}$$

where T_D summarizes terms containing geometric variations and B marks the extra sensitivity derivative terms resulting from the differentiation of the turbulence model.

In flow control optimization problems, the jet velocities do not affect the geometrical shape, *i.e.* $\delta x_k/\delta b_m = \delta n_i/\delta b_m = \delta t^l/\delta b_m = 0$, the total and partial derivatives coincide, and thus $T_D = 0$. In addition, the design variables b_m are the (hypothetical) normal jet volume fluxes applied to the surface of the duct to be optimized. On the discrete level, for the mth face on the solid (perforated) wall, with area ΔS_m, b_m is defined as $b_m = \Delta S_m v_{lm} n_{lm}$. Since ΔS_m is not varying, we get

$$\frac{\delta F}{\delta b_m} = \frac{1}{\Delta S_m}\frac{\delta F}{\delta v_{lm}} n_{lm}, \tag{26}$$

where $l = 1, 2(, 3)$ stands for the Cartesian velocity components and $m \in [1, N]$ is the boundary face index along the controlled body surface (no summation implied over m). The derivative w.r.t. the mth jet becomes

$$\frac{1}{\Delta S_m}\frac{\delta F}{\delta v_{lm}} n_{lm} = u_{\langle n\rangle m} v_{\langle n\rangle m} + 2\nu \frac{\partial u_{\langle n\rangle m}}{\partial n} - q_m + \frac{\partial F_{S_{W,k}}}{\partial v_{lm}} n_{km} n_{lm}. \tag{27}$$

It is interesting to note that, in flow control optimization problems, both T_D and B are absent, irrespective of the objective function used.

To summarize, by taking into account the variation in ν_t, extra terms appear in the field adjoint equations, their boundary conditions and the sensitivity derivative expression (for shape optimization problems). These are marked as *A1* (Equation 18), *A2* (Equation 24), and *B* (Equation 25).

4.5. *Sensitivities of the total pressure losses objective function*

The proposed continuous adjoint method is applied to the minimization of the volume-averaged total pressure losses between the inlet and outlet boundaries of Ω, given by

$$F_{p_t} = \int_{S_I} F_{S_{I,i}} n_i \,\mathrm{d}S + \int_{S_O} F_{S_{O,i}} n_i \,\mathrm{d}S = -\int_{S_I} \left(p + \frac{1}{2} v_m^2\right) v_i n_i \,\mathrm{d}S - \int_{S_O} \left(p + \frac{1}{2} v_m^2\right) v_i n_i \,\mathrm{d}S. \tag{28}$$

In shape optimization, since F is not defined along S_W, $T_D = 0$ and the sensitivity derivatives are given by

$$\begin{aligned}\frac{\delta F_{p_t}}{\delta b_m} = &-\int_{S_W} \left[\nu\left(\frac{\partial u_i}{\partial x_j} + \frac{\partial u_j}{\partial x_i}\right) n_j - q n_i\right] \frac{\partial v_i}{\partial x_k} n_k \frac{\delta x_l}{\delta b_m} n_l \,\mathrm{d}S \\ &- \int_{S_w} \nu \frac{\partial k_a}{\partial n}\frac{\partial k}{\partial n}\frac{\delta x_k}{\delta b_m} n_k \,\mathrm{d}S - \int_{S_w} \nu \frac{\partial \epsilon_a}{\partial n}\frac{\partial \epsilon}{\partial n}\frac{\delta x_k}{\delta b_m} n_k \,\mathrm{d}S.\end{aligned} \tag{29}$$

In flow control optimization problems, due to the zero Dirichlet condition imposed on u_i along S_W, Equation (27) becomes as simple as

$$\frac{1}{\Delta S_m}\frac{\delta F_{p_t}}{\delta v_{lm}} n_{lm} = 2\nu \frac{\partial u_{\langle n\rangle m}}{\partial n} - q_m. \tag{30}$$

5. Applications to shape and flow control optimization

In order to validate the proposed method and the programmed software for the computation of $\delta F/\delta b_m$ in incompressible flows governed by the Launder–Sharma k–ϵ model, three shape problems and a single active flow control optimization problem are investigated in Sections 5.1

and 5.2, respectively. Finally, the gain in the optimization process due to the differentiation of the turbulence model is investigated in Section 5.3. In all cases, F_{p_t} (Equation 28) is used as the objective function. In order to validate the accuracy of the sensitivities computed by the proposed method, comparisons are conducted with the outcome of either direct differentiation or finite differences ('reference' values).

5.1. *Validation in shape optimization problems*

The first case examined refers to the flow in an S-shaped duct. The flow Reynolds number, based on the inlet height, is equal to $\mathrm{Re} = 1.33 \times 10^4$. A structured grid with 200×160 nodes was generated; this was adequately stretched close to the solid walls to guarantee that, in the examined flow conditions, the non-dimensional distance y^+ of the first nodes off the wall was below 0.1. The computed primal and adjoint kinetic energy isolines are illustrated in Figures 1a and 1b, respectively; one may clearly observe the wake-like development of the k_a field upstream of the curved part of the lower wall. The shape control variables, b_m, w.r.t. which the sensitivity derivatives of F_{p_t} are computed, are the normal displacements of the wall grid nodes. Since only the grid nodes forming the S-shaped section are of interest, derivatives are computed w.r.t. these nodes only.

The sensitivity derivatives of F_{p_t} w.r.t. the control variables b_m are computed using three different methods:

(a) the proposed adjoint method that takes into account variations in the turbulence variables w.r.t. b_m,
(b) the adjoint method which relies upon the 'frozen turbulence' assumption, and
(c) the 'reference' method (DD).

The results are presented in Figure 2a. Due to the high cost of computing the 'reference' sensitivities, these are computed every 10 solid wall points; practically, there is no reason to perform more computations since the computed results are representative of the distribution of sensitivities. It can be observed that the results of the proposed method perfectly match the 'reference' ones, whereas those resulting from the 'frozen turbulence' assumption deviate from them.

The same conclusions about the significance of the turbulence model differentiation can also be reached in the second case examined; comparisons for a duct with a bump over its bottom surface are shown in Figure 2b. The flow Reynolds number, based on the inlet height, is $\mathrm{Re} = 4 \times 10^3$ and the structured grid consists of 200×160 nodes. Primal and adjoint turbulent energy dissipation contours are presented in Figures 3a and 3b, respectively.

A close-up view of the primal and adjoint velocity fields near the flow separation region is illustrated in Figure 4 for both cases. It can readily be observed that the transversal gradient of the adjoint velocity near the wall is greater than that of the primal velocity. To investigate the importance of this observation, three runs were conducted in each case, each one yielding a different average y^+ value. As shown in Figure 5, while the primal solution remains unchanged (the $C_p = 2(p - p_{\mathrm{in}})/v_{\mathrm{in}}^2$ curves practically coincide), the sensitivity derivatives are indeed affected. For instance, the computations on the coarser grids deviate from the results obtained using the stretched grids, due to the fact that the coarser grid resolution fails to capture the intense adjoint velocity gradient near the wall. It is thus concluded that only the two more stretched grids ensure grid independent gradient computations.

In Figures 6 and 7, the importance of the 'adjoint turbulence terms' in the adjoint mean flow equations ($A1$ in Equation 18), the adjoint outlet boundary conditions ($A2$ in Equation 24) and the sensitivity derivatives expression (B in Equation 25) is presented for the two aforementioned cases. Based on these comparisons, it can be concluded that $A2$ and B can even be omitted without

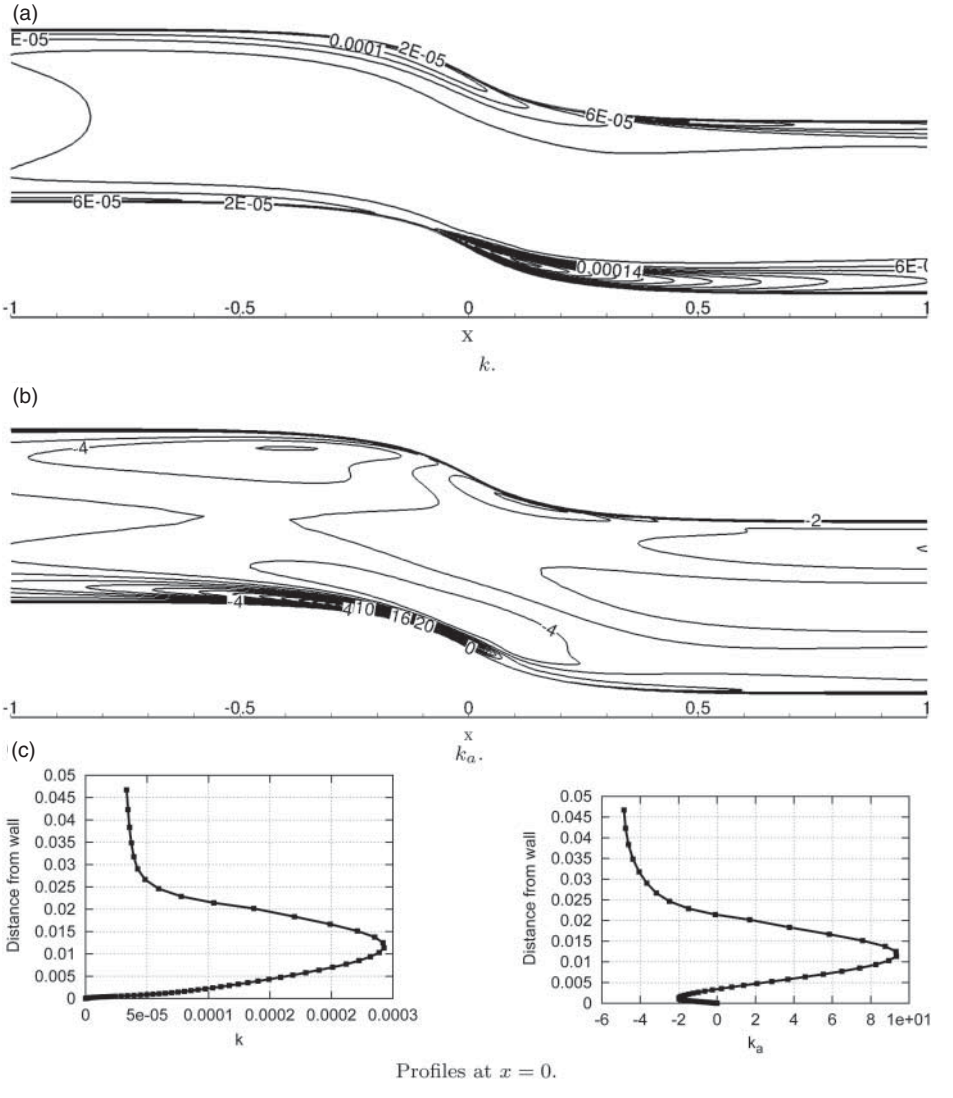

Figure 1. Case 1 (S-shaped duct). Primal (a) and adjoint (b) turbulent kinetic energy fields close to the curved part of the duct along with the the k, k_a profiles at $x = 0$ (c). The k_a upwind facing wake can be attributed to the negative sign in the convection term of R^{k_a} in Equation (19).

loss in accuracy, whereas $A1$ must surely be retained, since this term greatly affects the computed derivatives. It is interesting that the same behaviour was also observed in Zymaris *et al.* (2009) for the equivalent terms in the adjoint to the Spalart–Almaras turbulence model. This may lead to the conclusion that, if other turbulence models were differentiated, the terms that are likely to affect the sensitivity derivatives would still be those added to the adjoint momentum equations.

In Figure 8, a study regarding the deviation of the 'frozen turbulence' adjoint method from the proposed one, by focusing on the role of the flow Reynolds number, is presented. For this study, a third geometry, that of a 90° elbow duct with a constant cross sectional area, is used. Sensitivity derivatives of F_{p_t} w.r.t. the normal nodal displacement of the wall points are computed using the 'frozen' and 'full turbulence' adjoint methods, for two flow Reynolds numbers ($\mathrm{Re} = 7 \times 10^4$,

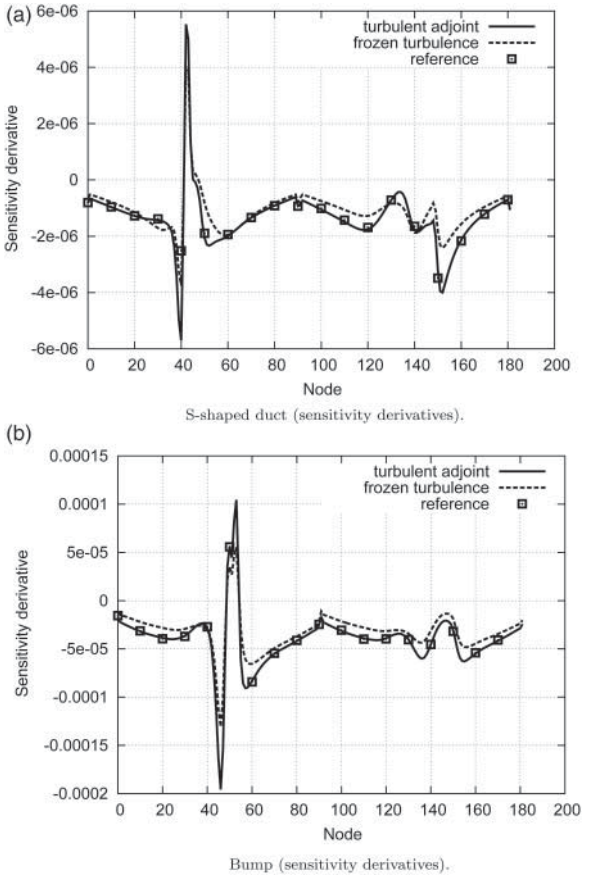

Figure 2. (a) Case 1 (S-shaped duct), and (b) Case 2 (bump). Sensitivity derivatives $\delta F_{p_t}/\delta b_m$, where b_m stand for the normal displacements of the solid wall grid nodes. The normal unit vector is facing from the fluid to the solid wall; negative sensitivity values indicate a displacement in this direction whereas positive values indicate an opposite favourable displacement. The abscissa stands for the nodal numbers. For both geometries, points numbered from 0 to 90 correspond to the lower duct walls whereas those numbered from 91 to 181 correspond to the upper one. Derivatives computed using the proposed continuous adjoint method (marked as 'turbulent adjoint'), and the adjoint method based on the 'frozen turbulence' assumption (marked as 'frozen turbulence') are compared to the 'reference' values (DD).

$\mathrm{Re} = 7 \times 10^5$). For fully turbulent flows, the loss in accuracy in the computed sensitivities caused by the 'frozen turbulence' assumption increases with Reynolds number.

5.2. *Validation in flow control optimization problems*

This section exploits further the adjoint to the Launder–Sharma k–ϵ turbulence model presented in Section 4. By solving the same field adjoint equations (Section 4.2) with the same boundary conditions (Section 4.3) as presented for shape optimization, information about the optimal jet location and 'type' can be extracted, by just post-processing the adjoint fields. The flow control sensitivity formula is given by Equation (27) and specialized for F_{p_t} in Equation (30).

A single but convincing test case is examined. It is important to note that the use of the 'frozen turbulence' assumption can lead to wrongly signed sensitivities and, therefore, mislead the designer during the selection of the most important jet parameters.

The proposed method is used to compute the sensitivity derivatives of F_{p_t} w.r.t. the (hypothetical) jet volume flow rate applied along the walls of an S-shaped duct. A 200×120 structured mesh

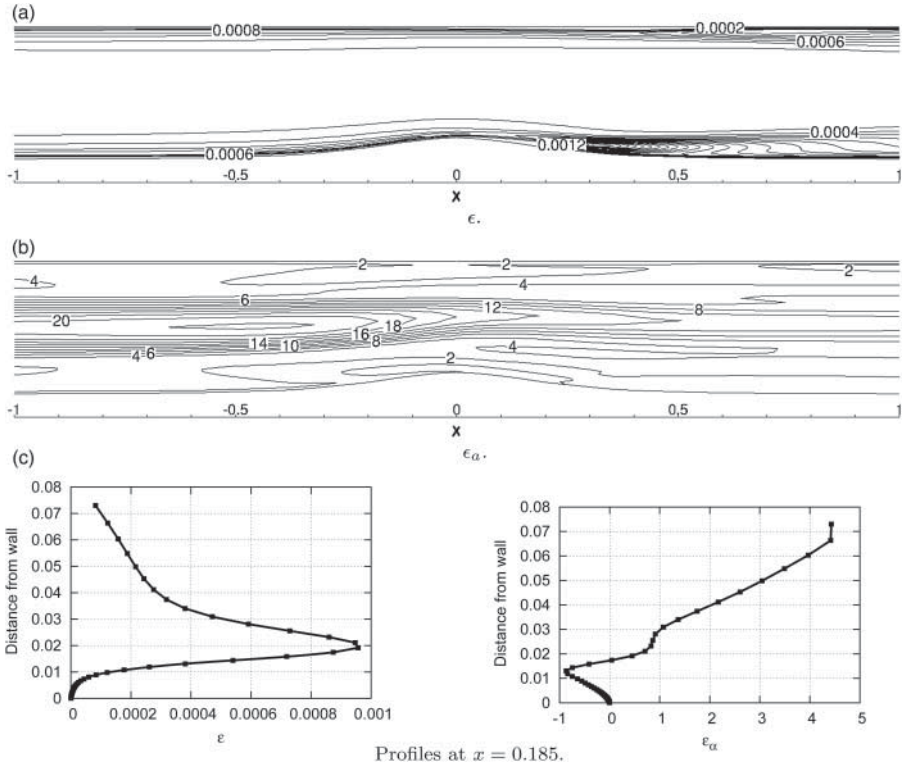

Figure 3. Case 2 (bump), close-up view near the bump-shaping. Primal (a) and adjoint (b) turbulent dissipation fields, along with the respective profiles at $x = 0.185$ (c). The adjoint quantity, ϵ_a, is convected upstream by the primal velocity, due to the minus sign in the convection term of R^{ϵ_a} in Equation (20).

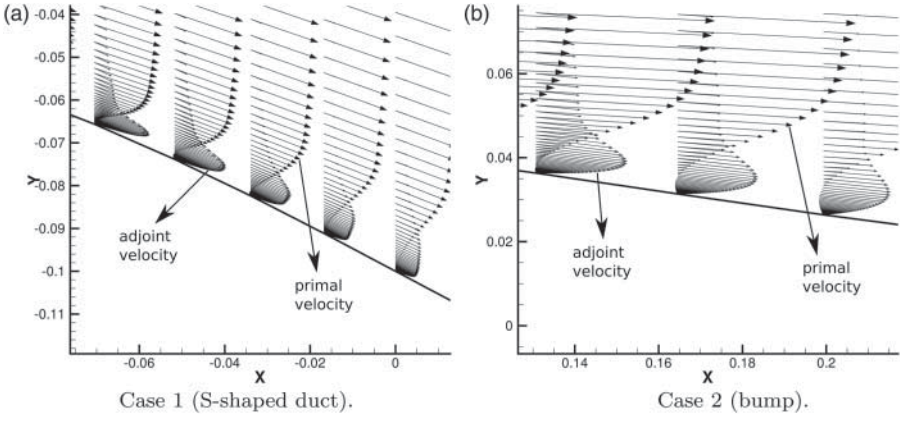

Figure 4. (a) Case 1 (S-shaped duct), and (b) Case 2 (bump). Primal and adjoint velocity vector fields near the separation region. The intense adjoint velocity gradient in the vicinity of the wall can be observed in both cases.

was used, with an average non-dimensional distance off the wall equal to $y^+ = 0.1$. The Reynolds number based on the inlet height is $\mathrm{Re} = 2.5 \times 10^4$. Adjoint pressure contours are presented in Figure 9.

In Figure 10, the sensitivities computed with the proposed method are compared to those obtained using the 'frozen turbulence' assumption and the 'reference' values (FD). The outcome

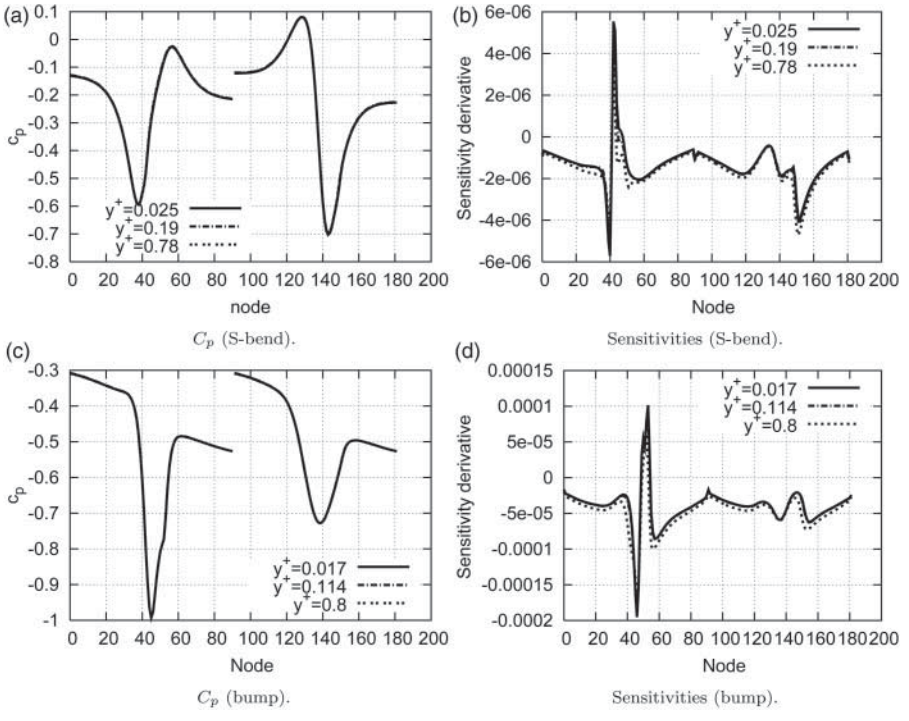

Figure 5. (a) and (b) Case 1 (S-shaped duct); (c) and (d) Case 2 (bump). (a) and (c): C_p distributions for the three differently stretched grids practically coincide. The three grids are characterized by the average y^+ value of the first row of cell centres. (b) and (d): sensitivity derivatives computed on the coarser grids are affected by the intense adjoint velocity gradient. Abscissa numbering as in Figure 2.

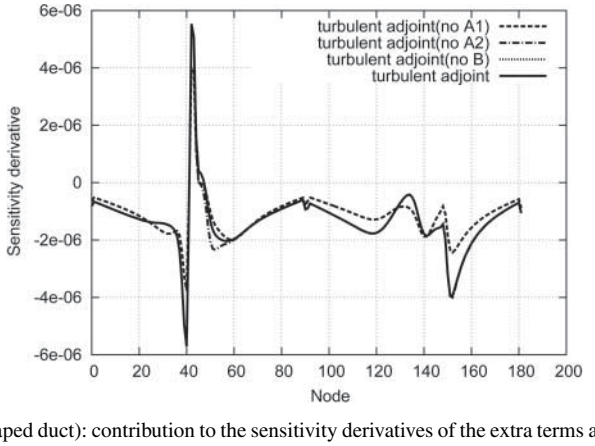

Figure 6. Case 1 (S-shaped duct): contribution to the sensitivity derivatives of the extra terms arising from the proposed turbulent adjoint approach. Abscissa numbering as in Figure 2. The extra terms, $A1$ (Equation 18), $A2$ (Equation 24) and B (Equation 25) are omitted, one at a time. Only the omission of $A1$, *i.e.* the extra term appearing in the adjoint momentum equations due to the differentiation of the turbulence model equations, seems to greatly affect the computed sensitivity derivatives. The omission of $A2$ slightly affects the sensitivities between nodes 40 to 60 while the omission of B does not significantly affect the sensitivities.

of the proposed method closely matches the reference values whereas the sensitivities computed using the 'frozen turbulence' assumption have the wrong sign along a significant part of S_W. This discrepancy is enough to mislead the flow control system designer and proves that the

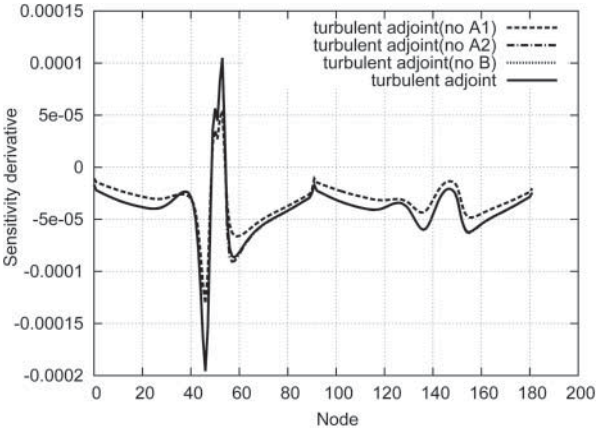

Figure 7. Case 2 (bump): contribution to the sensitivity derivatives of the extra terms arising from the proposed turbulent adjoint approach. Notation and conclusions as in figure 6.

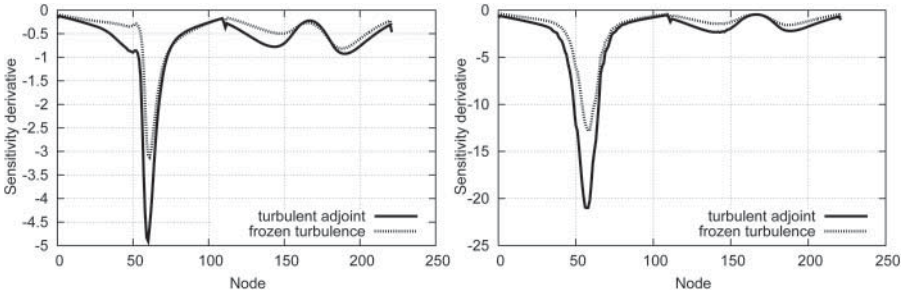

Figure 8. Case 3 (90° duct): sensitivity derivatives w.r.t. the normal displacement of the boundary nodes at two different Reynolds numbers, computed using (a) the proposed method and (b) the 'frozen turbulence' assumption. The first 110 nodes in the abscissa correspond to the inner radius of the duct whereas the last 110 correspond to the outer one. (a) $\mathrm{Re} = 7 \times 10^4$; (b) $\mathrm{Re} = 7 \times 10^5$. Tests performed for Reynolds numbers less than 10^3 showed that in those tests the turbulent adjoint and the 'frozen turbulence' assumption lead to almost identical results.

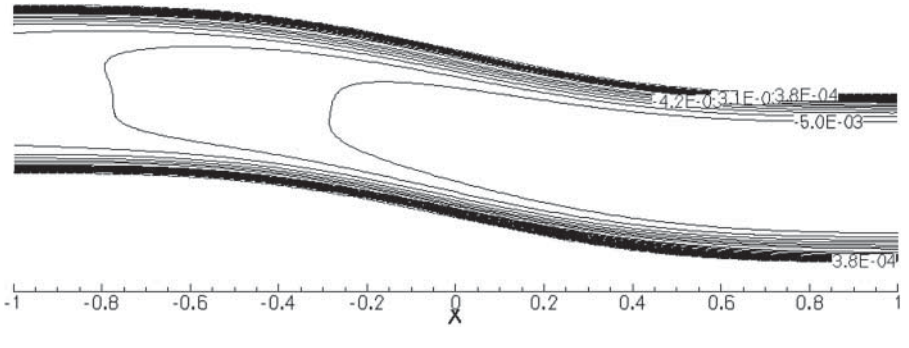

Figure 9. Flow control (S-shaped duct): adjoint pressure field, plotted close to the curved part of the duct.

differentiation of the turbulence model is essential (at least in some cases). According to Figure 10, suction should be applied to both the upper and, preferably, the lower duct contours in order to minimize viscous losses.

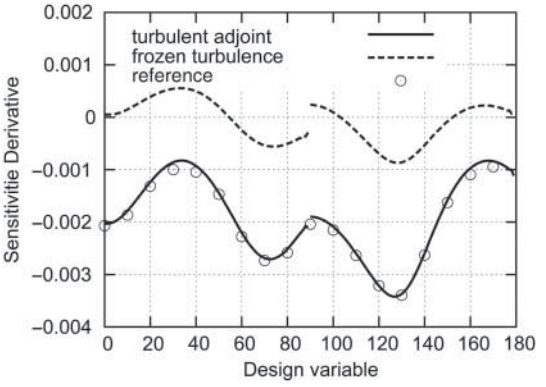

Figure 10. Flow control (S-shaped duct): F_{p_t} sensitivity derivatives w.r.t. the jet volume flow rate imposed on the surface of the duct. The abscissa stands for the boundary face numbers. The first 90 faces correspond to the upper duct wall whereas the last 90 correspond to the lower one. Positive sensitivity values indicate the local application of blowing in order to minimize F_{p_t} whereas negative values indicate suction. Derivatives are computed using (a) the proposed continuous adjoint method (marked as 'turbulent adjoint'), (b) the adjoint method based on the 'frozen turbulence' assumption (marked as 'frozen turbulence') and (c) the 'reference' method (FD). The proposed method recommends the use of suction for the entire duct surface, whereas results obtained making the 'frozen turbulence' assumption wrongly indicate some areas where blowing would be favourable.

5.3. *Expected gain in the optimization process*

In Sections 5.1 and 5.2, the gain in accuracy of the sensitivity derivatives achieved by the proposed method was demonstrated for shape and flow control optimization problems. In this section, dealing exclusively with shape optimization, the effect of the increased accuracy on the optimization process is quantified.

The shape optimization of an S-shaped duct targeting minimum total pressure losses is investigated. The structured mesh used consists of 210×250 nodes. The flow Reynolds number based on the inlet height is $\mathrm{Re} = 1.2 \times 10^5$. The upper and lower duct contours are parameterized using Bézier–Bernstein polynomials with 12 control points each, Figure 11.

Two gradient-based optimization methods, namely steepest descent and the Fletcher–Reeves Conjugate Gradient (CG) method (Fletcher and Reeves 1964), are utilized. The gradients used by each method to update the design variables are based on (a) the proposed method to compute $\delta F_{p_t}/\delta b_m$ and (b) the adjoint method with the 'frozen turbulence' assumption. Within each optimization cycle, the algorithmic steps for updating the design variables are listed below.

(1) Solve the flow equations, Equations (1) and (2).
(2) Compute F_{p_t} through Equation (28) and apply the stopping criterion.
(3) Solve the adjoint equations, Equations (17) to (20), along with appropriate boundary conditions, Section 4.3.
(4) Compute $\delta F_{p_t}/\delta b_m$ using Equation (29).
(5) Update the design variables, $\mathbf{b}^{k+1}$.
(6) Update the computational mesh.
(7) Go to step 1.

The algorithm based on the 'frozen turbulence' assumption differs only in step 3, where the extra terms and PDEs emerging from the differentiation of the turbulence model are not considered. In order to have a fair comparison between the convergence rates of the optimization variants (a) and (b), the correction step is adapted to give a maximum boundary deformation of 2.5×10^{-2} in the first optimization cycle, for each of them.

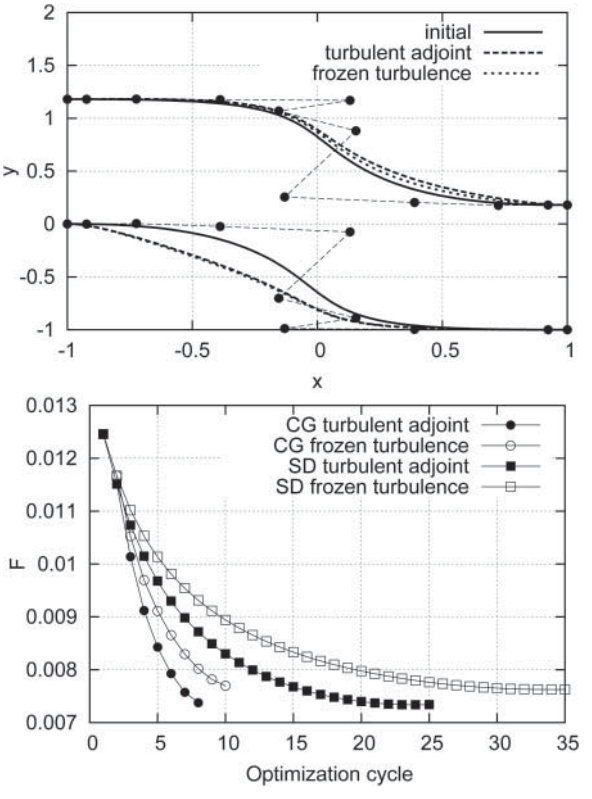

Figure 11. Optimization studies (S-shaped duct): shape optimization of an S-shaped duct targeting minimum F_{p_t}, based on two different optimization algorithms. Top: starting duct shape compared to the optimal solutions resulting from the steepest descent algorithm that uses (a) the proposed method to compute $\delta F_{p_t}/\delta b_m$ (labelled 'turbulent adjoint') and (b) the adjoint method based on the 'frozen turbulence' assumption (labelled 'frozen turbulence'); axes not in scale. Both variants reach approximately the same optimal solutions. Each of the lower and upper duct curved walls is parameterized using Bézier–Bernstein polynomials with 12 control points. Only the y coordinates of the control points are allowed to vary during the optimization process, giving rise to a problem with 24 design variables. Bottom: convergence history of two optimization algorithms – Steepest Descent (SD)and Conjugate Gradient (CG) – driven by different adjoint methods. The algorithms based on the exact differentiation of the Launder–Sharma k–ϵ turbulence model need at least 20% fewer cycles to reach the minimum F value.

The starting shape of the duct along with the optimal ones computed by the steepest descent method, based on the two variants of the adjoint formulation, are presented in Figure 11(a). Both variants have reached practically the same result. The geometry resulting from variant (a) has an objective function value that is about 3% lower than that of variant (b). Moreover, the variant that uses the proposed adjoint method to compute the sensitivity derivatives reaches the optimal solution after approximately 30% fewer cycles than that using the 'frozen turbulence' assumption. The beneficial impact of the fully differentiated turbulence model on the optimization procedure is reconfirmed for optimization algorithms based on the CG method, Figure 11(b). The same optimization problem is solved using the Fletcher–Reeves CG method and a 20% economy in optimization cycles is observed when using exact sensitivity derivatives.

6. Conclusions

A continuous adjoint formulation for shape and active flow control optimization problems governed by the incompressible turbulent flow equations and the low-Re number Launder–Sharma

k–ϵ turbulence model has been presented. The differentiation of the turbulence model equations leads to extra terms in the adjoint momentum equations, their boundary conditions and the sensitivity derivatives. Regarding shape optimization problems, it seems that, in practice only the terms appearing in the adjoint momentum equations affect the computed sensitivity derivatives, whereas the rest could even be neglected. Similar results were presented in Zymaris *et al.* (2009) for the differentiation of the low-Re number Spalart–Allmaras model, indicating that these observations can possibly be generalized to other turbulence models as well. Based on the studies conducted, the adjoint equations require a finer computational mesh close to the wall boundaries in order to reach mesh-independent results (compared to what is required for the primal problem). The sensitivities computed using the proposed method closely match the reference values, computed either with direct differentiation or finite differences, for shape and flow control optimization problems. Especially in the case of flow control optimization, sensitivities computed using the 'frozen turbulence' assumption are wrongly signed, which could seriously mislead the designer. Finally, the gain in the optimization procedure caused by the differentiation of the turbulence model was quantified. Two variants of gradient-based optimization algorithms were examined, making use of sensitivity derivatives computed using either the proposed approach (algorithm (a)) or the adjoint approach based on the 'frozen turbulence' assumption (algorithm (b)). For the shape optimization examined of an S-shaped duct, algorithm (a) outperformed algorithm (b) by more than 20%, for optimization procedures based on either steepest descent or the conjugate gradient method.

Acknowledgements

This research was conducted in association with ICON Technology and Process Consulting (UK) Ltd. The methods presented in this article are implemented using technology based upon OpenFOAM®[1] and made available within the CFD service ICON FOAMpro, http://www.iconcfd.com/foampro.

Note

1. OpenFOAM® is a CFD Toolbox produced by OpenCFD Ltd and distributed by the OpenFOAM Foundation.

References

Anderson, W. K., and D. L. Bonhaus. 1999. "Airfoil Design on Unstructured Grids for Turbulent Flows." *AIAA Journal* 37 (2): 185–191.

Anderson, W. K., and V. Venkatakrishnan. 1999. "Aerodynamic Design Optimization on Unstructured Grids with a Continuous Adjoint Formulation." *Computers & Fluids* 28 (4–5): 443–480.

Bueno-Orovio, A., C. Castro, F. Palacios, and E. ZuaZua. 2012. "Continuous Adjoint Approach for the Spalart–Allmaras Model in Aerodynamic Optimization." *AIAA Journal* 50 (3): 631–646.

Burgreen, G. W., and O. Baysal. 1996. "Three-Dimensional Aerodynamic Shape Optimization Using Discrete Sensitivity Analysis." *AIAA Journal* 34 (9): 1761–1770.

Carnarius, Angelo, Frank Thiele, Emre Özkaya, Anil Nemili, and Nicolas R. Gauger. 2013. "Optimal Control of Unsteady Flows Using a Discrete and a Continuous Adjoint Approach." *System Modeling and Optimization, IFIP Advances and Communication Technology* 391: 318–327.

Cathalifaud, P., and P. Luchini. 2000. "Algebraic Growth in Boundary Layers: Optimal Control by Blowing and Suction at the Wall." *European Journal of Mechanics-B/Fluids* 19 (4): 469–490.

Collis, S. Scott, Ronald D. Joslin, Avi Seifert, and Vassilis Theofilis. 2004. "Issues on Active Flow Control: Theory, Control, Simulation and Experiment." *Progress in Aerospace Sciences* 40 (4–5): 237–289.

Duta, M. C., M. B. Giles, and M. S. Campobasso. 2002. "The Harmonic Adjoint Approach to Unsteady Turbomachinery Design." *International Journal for Numerical Methods in Fluids* 40 (3–4): 323–332.

Dwight, R., J. Brézillon, and D. Vollmer. 2006. "Efficient Algorithms for Solution of the Adjoint Compressible Navier–Stokes Equations with Applications." Paper presented at the 7th ONERA-DLR Aerospace Symposium (ODAS), Toulouse, October 4–6.

Elliott, J., and J. Peraire. 1996. "Aerodynamic Design Using Unstructured Meshes." Paper presented at the 27th AIAA Fluid Dynamics Conference, New Orleans, LA, June 17–20. doi:10.2514/6.1996-1941.

Fletcher, R., and C. M. Reeves. 1964. "Function Minimization by Conjugate Gradients." *Computer Journal* 7 (2): 149–154.

Giles, M. B., and N. A. Pierce. 1997. "Adjoint Equations in CFD: Duality, Boundary Conditions and Solution Behaviour." Paper presented at the 13th AIAA Computational Fluid Dynamics Conference, Snowmass Village, CO, June 29–July 2. doi:10.2514/6.1997-1850.

Giles, M., and N. Pierce. 2000. "An Introduction to the Adjoint Approach to Design." *Flow, Turbulence and Combustion* 65: 393–415.

Grinfield, P. 2010. "Hadamard's Formula Inside and Out." *Journal of Optimization Theory and Applications* 146 (3): 654–690.

He, J. W., M. Chevalier, R. Glowinski, R. Metcalfe, A. Nordlander, and J. Periaux. 2000. "Drag Reduction by Active Control for Flow Past Cylinders." *Computational Mathematics Driven by Industrial Problems* 1739: 287–363.

Jameson, A. 1988. "Aerodynamic Design Via Control Theory." *Journal of Scientific Computing* 3 (3): 233–260.

Jameson, Antony, and Juan J. Alonso. 1996. "Automatic Aerodynamic Optimization on Distributed Memory Architectures." Paper presented at the 34th AIAA Aerospace Sciences Meeting and Exhibit, Reno, NV, January 8–12. AIAA Paper Number 96-0409. http://aero-comlab.stanford.edu/Papers/reno96.pdf.

Jameson, A., N. Pierce, and L. Martinelli. 1998. "Optimum Aerodynamic Design Using the Navier–Stokes equations." *Theoretical and Computational Fluid Dynamics* 10: 213–237.

Joslin, R. D., M. D. Gunzburger, R. A Nicolaides, G. Erlebacher, and M. Y. Hussaini. 1997. "Self-Contained Automated Methodology for Optimal Flow Control." *AIAA Journal* 35 (5): 816–824.

Launder, B. E., and B. I. Sharma. 1974. "Application of the Energy-Dissipation Model of Turbulence to the Calculation of Flow near a Spinning Disc." *Letters in Heat and Mass Transfer* 1 (2): 131–137.

Lee, B. J., and C. Kim. 2007. "Automated Design Methodology of Turbulent Internal Flow Using Discrete Adjoint Formulation." *Aerospace Science and Technology* 11 (2–3): 163–173.

Li, Zhijin, I. M. Navo, M. Y. Hussaini, and F. X. Le Dimet. 2003. "Optimal Control of Cylinder Wakes Via Suction and Blowing." *Computers & Fluids* 32 (2): 149–171.

Mishra, A., K. Mani, D. Mavriplis, and J. Sitaraman. 2013. "Time Dependent Adjoint-Based Optimization for Coupled Aeroelastic Problems." Presented at the 31st AIAA Applied Aerodynamics Conference, San Diego, CA. doi:10.2514/6.2013-2906.

Nadarajah, Siva, and Antony Jameson. 2001. "Studies of the Continuous and Discrete Adjoint Approaches to Viscous Automatic Aerodynamic Shape Optimization." Paper presented at the 15th AIAA Computational Fluid Dynamics Conference, Anaheim, June 11–14. doi:10.2514/6.2001-2530.

Nadarajah, S., and A. Jameson. 2002. "Optimal Control Theory of Unsteady Flows Using a Time Accurate Method." Presented at the 9th AIAA/ISSMO Symposium on Multidisciplinary Analysis and Optimization, Atlanta, GA, September 4–6. doi:10.2514/6.2002-5436.

Naumann, Uwe. 2012. *The Art of Differentiating Computer Programs: An Introduction to Algorithmic Differentiaion*. Philadelphia, PA: SIAM.

Nemili, A., E. Özkaya, N. R. Gauger, F. Kramer, A. Carnarius, and F. Thiele. 2013. "Discrete Adjoint Based Sensitivity Analysis for Optimal Flow Control of a 3D High-Lift Configuration." Presented at the 21st AIAA Computational Fluid Dynamics Conference, San Diego, CA, June 24–27. doi:10.2514/6.2013-2585.

Nielsen, E. J., J. Lu, M. A. Park, and D. L. Darmofal. 2004. "An Implicit Exact Dual Adjoint Solution Method for Turbulent Flows on Unstructured Grids." *Computers & Fluids* 33 (9): 1131–1155.

Othmer, C. 2008. "A Continuous Adjoint Formulation for the Computation of Topological and Surface Sensitivities of Ducted Flows." *International Journal for Numerical Methods in Fluids* 58 (8): 861–877.

Papadimitriou, D. I., and K. C. Giannakoglou. 2007. "A Continuous Adjoint Method with Objective Function Derivatives Based on Boundary Integrals for Inviscid and Viscous Flows." *Journal of Computers & Fluids* 36 (2): 325–341.

Papadimitriou, D. I., and K. C. Giannakoglou. 2012. "Aerodynamic Design Using the Truncated Newton Algorithm and the Continuous Adjoint Approach." *International Journal for Numerical Methods in Fluids* 68 (6): 724–739.

Patankar, S. V., and D. B. Spalding. 1972. "Calculation Procedure for Heat, Mass and Momentum Transfer in Three-dimensional Parabolic Flows." *International Journal of Heat and Mass Transfer* 15 (10): 1787–1806.

Pironneau, O. 1984. *Optimal Shape Design for Elliptic Systems*. New York: Springer-Verlag.

Pralits, J. O., A. Hanifi, and D. S. Henningson. 2002. "Adjoint-Based Optimization of Steady Suction for Disturbance Control in Incompressible Flows." *Journal of Fluid Mechanics* 467: 129–161.

Prandtl, L. 1904. "Über Flüssigkeitsbeweung bei sehr kleiner Reibung." In *Proceedings of the 3rd International Mathematical Congress*, Heidelberg, 484–491. Teuber Verlag, Leipzig.

Reuther, J., J. J. Alonso, M. J. Rimlinger, and A. Jameson. 1996. "Aerodynamic Shape Optimization of Supersonic Aircraft Configurations Via an Adjoint Formulation on Distributed Memory Parallel Computers." Presented at the 6th AIAA/NASA/ISSMO Symposium on Multidisciplinary Analysis and Optimization, Bellevue, WA, September 4–6. doi:10.2514/6.1996-4045.

Taylor, T. W. R., F. Palacios, K. Duraisami, and J. J. Alonso. 2013. "A Hybrid Adjoint Approach Applied to Turbulent Flow Simulations." Presented at the 21st AIAA Computational Fluid Dynamics Conference, San Diego, CA, June 24–27. doi:10.2514/6.2013-2452.

Zhang, Z., P. C. Chen, S. Yang, Z. Wang, and Q. Wang. 2013. "Unsteady Aero-Structure Coupled Adjoint Method for Flutter Suppression." Presented at the 21st AIAA Computational Fluid Dynamics Conference, San Diego, CA, June 24–27. doi:10.2514/6.2013-2849.

Zymaris, A. S., D. I. Papadimitriou, K. C. Giannakoglou, and C. Othmer. 2009. "Continuous Adjoint Approach to the Spalart–Allmaras Turbulence Model for Incompressible Flows." *Computers & Fluids* 38 (8): 1528–1538.
Zymaris, A. S., D. I. Papadimitriou, K. C. Giannakoglou, and C. Othmer. 2010. "Adjoint Wall Functions: A New Concept for Use in Aerodynamic Shape Optimization." *Journal of Computational Physics* 229 (13): 5228–5245.
Zymaris, A. S., D. I. Papadimitriou, E. M. Papoutsis-Kiachagias, K. C. Giannakoglou, and C. Othmer. 2013. "The Continuous Adjoint Method as a Guide for the Design of Flow Control Systems Based on Jets." *Engineering Computations* 30 (4): 494–520.